Frontiers of Physics
https://doi.org/10.1007/s11467-019-0903-6
Front. Phys.
14(5), 53402 (2019)

REVIEW ARTICLE

Rational design of photoelectrodes for photoelectrochemical water splitting and CO_2 reduction

Yu Hui Lui*, Bowei Zhang*, Shan Hu†

Department of Mechanical Engineering, Iowa State University, Ames, IA 50011, USA
Correspondence author. E-mail: †shanhu@iastate.edu
Received March 17, 2019; accepted April 16, 2019

Solar energy has promising potential for building sustainable society. Conversion of solar energy into solar fuels plays a crucial role in overcoming the intermittent nature of the renewable energy source. A photoelectrochemical (PEC) cell that employs semiconductor as photoelectrode to split water into hydrogen or fixing carbon dioxide (CO_2) into hydrocarbon fuels provides great potential to achieve zero-carbon-emission society. A proper design of these semiconductor photoelectrodes thus directly influences the performance of the PEC cell. In this review, we investigate the strategies that have been put towards the design of efficient photoelectrodes for PEC water splitting and CO_2 reduction in recent years and provide some future design directions toward next-generation PEC cells for water splitting and CO_2 reduction.

Keywords photoelectrochemistry, water splitting, CO_2 reduction

Contents

1 Introduction

Global warming, as a result of anthropogenic emission of greenhouse gases [e.g., carbon dioxide (CO_2)], has led to increasing efforts in renewable energy researches and utilizations. Among all the renewable energy sources, solar energy is very attractive as it is the largest renewable source (with ~120 000 TW reaches the Earth's surface) [1, 2]. However, like many other renewable energy sources, solar energy is intermittent and variate diurnally and geographically. Hence, finding efficient and reliable methods to store solar energy is crucial for meeting daily energy demands.

Artificial photosynthesis is a promising and attractive approach to convert solar energy into energy-rich chemical fuels through processes such as water splitting, which generates hydrogen fuel, and CO_2 reduction, which fixes CO_2 into valuable chemicals. Hydrogen fuel can release energy with H_2O as the only byproduct, which is environmentally benign [1–5]. On the other hand, turning CO_2 into valuable chemicals with solar energy can decrease the atmospheric level of CO_2 and achieve carbon neutrality. There are three general routes available for the artificial photosynthesis: i) Photovoltaic cell combined with electrolysis cell; ii) photocatalytic cell; iii) photoelectrochemical (PEC) cell [2, 6–8]. Each route has its own merits and challenges. In this review, we will mainly focus on PEC cell.

Ever since the pioneering works by Fujishima and colleagues [9, 10], PEC cell has been widely explored in the

*These authors contributed equally. Special Topic: Solar Energy Storage and Applications (Eds. Min Liu and Haotian Wang).

endeavor of finding more efficient water splitting and CO_2 reduction strategies [1, 3, 11–13]. In a PEC cell configuration, the semiconductor is either directly in contact with the electrolyte to form a semiconductor-liquid junction (SCLJ) or separated from the electrolyte by an overlayer with versatile functionalities [13]. Such a cell configuration provides potential cost saving compared with Route 1, as PEC waives the need for an electrolysis cell and thus avoids the fabrication and assemble costs of two-individual cell (photovoltaic cell and electrolysis cell). Besides, unlike a photovoltaic cell which requires p–n junction, PEC cell comes with build-in electric field at the SCLJ. Thus, the SCLJ can drive photo-generated holes (electrons) to the photoanode (photocathode) surface for oxidation (reduction) reaction. Another benefit of PEC cell is the oxidation and reduction products are generated at two photoelectrodes, which can avoid products mixing as it is the case for Route 2. Despite the advantages, many researchers have pointed out that materials requirements for artificial photosynthesis are stringent. As the source of power for artificial photosynthesis is coming from the sunlight that reaches the earth surface (~0.1 $W{\cdot}cm^{-2}$ at most), the current density at the PEC electrodes is limited to the order of 10 $mA{\cdot}cm^{-2}$. This is far from the output for a commercial electrolyzer (~0.5–2 $A{\cdot}cm^{-2}$). This means that a PEC system needs to have an electrode size that is 50–200 times larger than that of a commercial electrolyzer [1, 14]. Thus, the use of cheap, abundant, and stable electrode material for PEC is necessary. Besides, any system with liquid is subjected to the risk of leakage, hence environmentally benign materials for PEC cell are also required.

This review focuses on the recent design strategies of PEC photoelectrode. Different strategies have been used in improving the performance of PEC photoelectrode in water splitting and CO_2 reduction. These strategies include the selection of underlying semiconductor, nanostructuring the semiconductor, applying cocatalyst layer(s) to enrich the semiconductor photocatalytic performance, or doping the semiconductor with different elements. We will first introduce the fundamentals in PEC cell, then review the photoelectrode designs in water splitting and subsequently CO_2 reduction. The intention of the arrangement is to slowly build up the readers' understanding in PEC system through a much simpler water splitting then move forward to CO_2 reduction.

2 Fundamentals of PEC in water splitting and CO_2 reduction

The process of splitting water molecule into hydrogen and oxygen is a thermodynamically uphill process as shown in Eq. (1). The free energy change for the reaction under standard conditions is $\Delta G = 237.2\ kJ{\cdot}mol^{-1}$. Using Nernst equation, we can calculate the reversible potential difference of the process to be $\Delta E^\circ = 1.23$ V per electron transferred. Ideally, a semiconductor requires a bandgap of at least 1.23 eV to drive the water splitting reaction, which can be translated into solar radiation with wavelengths shorter than ~1000 nm is needed. If the charge transfer resistance is taken into account, semiconductor with ~1.6-2.4 eV bandgap is required [3].

The overall water splitting reaction is the combination of two half-cell reactions, with one the oxygen evolution reaction (OER) and the other the hydrogen evolution reaction (HER):

$$\begin{aligned}
&H_2O + 2(h^+) \rightarrow \frac{1}{2}O_2 + 2H^+ \quad \text{(OER)}, && E^\circ_{OER} = -1.23\ \text{V vs. NHE},\\
&2H^+ + 2e^- \rightarrow H_2 \quad \text{(HER)}, && E^\circ_{HER} = 0.00\ \text{V vs. NHE},\\
&H_2O \rightarrow H_2 + \frac{1}{2}O_2 && \Delta E^\circ = -1.23\ \text{V}.
\end{aligned} \tag{1}$$

Standard electrode potential E° (under room temperature and pressure at pH 0) of each of the half reactions can be converted into electrochemical potential, which is given by $-qE^\circ$, where q is the elementary charge. Spontaneous PEC cell reaction requires the conduction band (CB) of the semiconductor to be located more negative than E°_{HER} and the valence band (VB) to be located more positive than E°_{OER} (shown in Fig. 1).

To reduce CO_2 in a PEC cell, water oxidation reaction is necessary to provide proton (H^+) to the photocathode to generate various products [as shown in Eqs. (1) and (2)]. The thermodynamic potential of CO_2 reduction to various products with respective to NHE under pH 7 conditions (at room temperature and pressure) are listed in Eq. (2):

$$\begin{aligned}
&2H^+ + 2e^- \rightarrow H_2, && E = -0.41\ \text{V},\\
&CO_2 + e^- \rightarrow CO_2^{*-}, && E = -1.85\ \text{V},\\
&CO_2 + 2H^+ + 2e^- \rightarrow CO + H_2O, && E = -0.52\ \text{V},\\
&CO_2 + 2H^+ + 2e^- \rightarrow HCO_2H, && E = -0.61\ \text{V},\\
&CO_2 + 4H^+ + 4e^- \rightarrow HCOH + H_2O, && E = -0.48\ \text{V},\\
&CO_2 + 6H^+ + 6e^- \rightarrow CH_3OH + H_2O, && E = -0.39\ \text{V},\\
&CO_2 + 8H^+ + 8e^- \rightarrow CH_4 + 2H_2O, && E = -0.24\ \text{V}.
\end{aligned} \tag{2}$$

As we can see from these reduction potentials, thermodynamically, the reduction of proton to hydrogen is very close to the reduction of carbon dioxide. Therefore, selectivity of the photoelectrocatalyst used in the process is very important [15]. Note that the difference between the standard reduction potential and the reduction potential

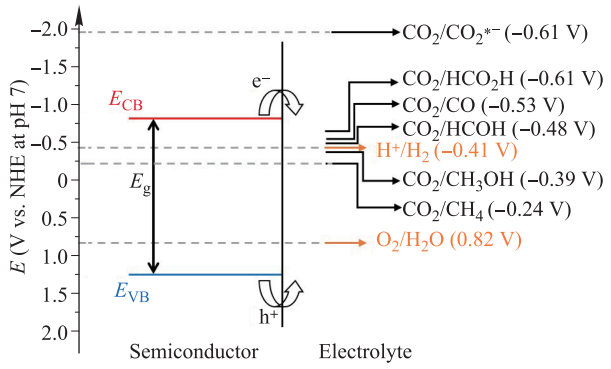

Fig. 1 Favorable conduction band (CB) and valence band (VB) energy levels for spontaneous oxidation of water and reduction of H^+ and most of the CO_2 reactions.

from proton to hydrogen under pH 7 follows Nernst relation: $E = E^\circ - 0.059x$, where x is the value of pH value of the solution. Similar to the band alignment in PEC for water splitting, the conduction band of a photoelectrode for a CO_2 reduction reaction needs to be lower than the reduction reaction potential (See Fig. 1) and the valence band needs to be higher than the oxidation reaction potential.

Photon energy larger than the bandgap (E_g) is required to excite an electron–hole pair in the semiconductor. Separation of the electron–hole pairs before the electron–hole recombination is crucial to improve the efficiency of the photocurrent density from a PEC cell. Unlike a photovoltaic device that requires a p–n junction to drive the separation of electron–hole pairs, PEC device exhibits a build-in electric field at the semiconductor-liquid junction (SCLJ). The build-in electric field is a result of the equilibration of electrochemical potential (Fermi level E_F) between the semiconductor and the redox couples of interests in the solution that leave a space charge region within the semiconductor surface. This space charge region also causes the electronic band of the semiconductor to bend (see Fig. 2). Once the electron–hole pairs have been separated, transfer of the charge carriers away from the surface of the semiconductor to the solution to participate in redox reactions is another crucial research topic in PEC cell. Many researches have been focusing on improving the charge separation efficiency and charge injection efficiency through nanostructuring, overlayer film deposition, p–n junction formation and dopant introduction into the semiconductor [3]. Detailed mechanisms of the SCLJ are not shown here. Interested reader can refer to Nozik and Memming's paper [16].

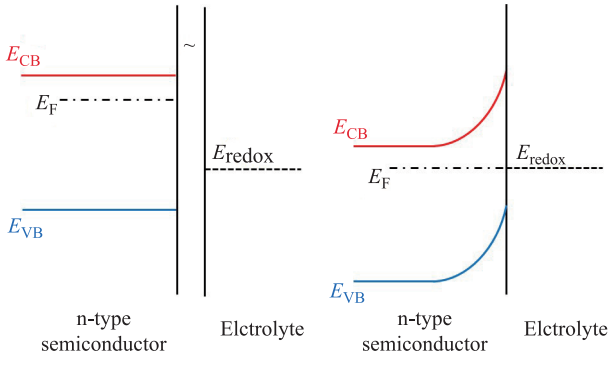

Fig. 2 Band bending at the n-type semiconductor-liquid junction (SCLJ).

3 Performance characterization

- Incident photon to current efficiency (IPCE)

IPCE quantifies the ratio of incident photon that are converted into electrons collected by the PEC cell at different wavelength of the incident light:

$$\mathrm{IPCE}(\lambda) = \frac{\text{collected electrons}}{\text{incident photons}} = \frac{J_{PEC}(\lambda)/e}{P_{mono}(\lambda)\left(\frac{hc}{\lambda}\right)} = \frac{J_{ph}(\lambda) \times 1239.8}{P_{mono}(\lambda) \times \lambda},$$

where $J_{PEC}(\lambda)$ (mA·cm^{-2}) is the photocurrent density of the PEC cell measured under monochromatic illumination at wavelength λ (nm), with power intensity $P_{mono}(\lambda)$ (mA·cm^{-2}), e (C) is the charge of one electron, h (J·s) is Planck's constant, c (m·s^{-1}) is the speed of light, and hc/e is equal to 1239.8 V·nm.

- Absorbed photon-to-current conversion efficiency (APCE)

When we want to know how much of the absorbed photon (instead of incident) is being converted into electron by the PEC cell, a charge generation efficiency term, $\eta_{e-/h+}$, i.e., ratio of incident photon that can be utilized by the PEC cell. $\eta_{e-/h+}$ can be estimated by using UV/Vis spectroscopy.

$$APCE(\lambda) = IPCE(\lambda)/\eta_{e^-/h^+}.$$

4 Photoelectrodes for solar water splitting

The design of photoelectrode is crucial to enable the commercialization of PEC water splitting cell. Many factors must be considered into a successful photoelectrode design. A PEC cell often operates under rather corrosive environments, i.e., for photoanode, basic electrolytes were often used, and for photocathode, acidic electrolytes were used instead. It is known that some semiconductor materials can degrade under extreme pH condition. For reliable long-term application, these semiconductor materials must be stable under solar radiation and acid/alkaline conditions.

Transition metal oxides have long been used in solar water splitting research since the pioneering work by Fujishima and colleagues [9], due to their stability and

environment-friendly nature. Popular transition metal oxides used in a PEC water splitting cells include n-TiO_2, n-WO_3, n-Fe_2O_3, n-$BiVO_4$, n-ZnO, p-CuO, p-Cu_2O, and p-NiO. Each material has its shortcomings and these shortcomings have been addressed in several reports. In this section, we will review the strategies that have been used in recent years to improve the PEC performance and stability of a few selected transition metal oxides.

4.1 Photoanodes

4.1.1 TiO_2 photoanode

Titanium dioxide (TiO_2), an n-type semiconductor with a bandgap ~3.2 eV [17–20], is widely used in PEC water splitting research since Fujishima's work in 1972 [9], mainly due to its high photostability, non-toxicity, abundancy, and low cost. However, the wide bandgap limits its ability to utilize visible light and the low charge carrier mobility will induce electron–hole recombination.

Nanostructuring TiO_2 photoelectrode to increase the surface-to-volume ratio has been a popular method to enhance the PEC performance. One-dimensional (1D) nanostructures have drawn many attentions due to the potential ability to provide fast electron transport pathway along the longitudinal direction. Anodized TiO_2 nanotubes [Figs. 3(a) and (b)] were reported by Grimes's group for solar water splitting [21, 22]. The length, the wall thickness, and the spacing of the highly ordered TiO_2 nanotube arrays grew on Ti foils can be adjusted by tuning the applied potential and chemical bath temperature. The optimized TiO_2 nanotube was able to achieve 6.8% photoconversion efficiency. Kim *et al.* demonstrated that the performance of the nanotubes can be improved by growing nano-branch layer on the side-walls of the nanotubes [23]. The nano-branch was a result of $TiCl_3$ solution treatment at 80 °C on the surface of TiO_2 nanotubes. The surface treatment was also shown to create oxygen vacancies on the surface of the nanotubes, which can enhance the charge transport efficiency by increasing the donor concentration. The nano-branch layer enhances the charge transfer efficiency by providing additional active sites for water adsorption. Besides 1D nanostructure, two-dimensional (2D) nanostructures have also shown promising results. Butburee *et al.* synthesized a 2D anatase TiO_2 porous single-crystalline nanostructure (PSNs) on FTO for PEC water splitting through an ion exchange-induced pore-forming process [Figs. 3(c) and (d)] [18]. The single crystalline nature of the nanostructure allows long-range charge diffusion length and structural coherence; the porous nature of the nanostructure allows abundant active sites for chemical reaction. The TiO_2 PSNs exhibit very low onset potential and a photocurrent density of 1.02 $mA{\cdot}cm^{-2}$ at 1.23 V vs. RHE (denoted as V_{RHE} hereafter), which is close to the theoretical limit of TiO_2 (1.12 $mA{\cdot}cm^{-2}$). One other popular strategy to improve the surface area is "host and guest" composite photoelectrode [19, 20]. Wang *et al.* constructed a 3D FTO inverse opal nanocrystal as conductive host for atomic layer deposited TiO_2 using polystyrene opals [Figs. 3(e) and (f)] [19]. The highly porous host provides a shorter pathway for photogenerated charge carriers from the TiO_2 photoelectrode. This work demonstrated a way to improve PEC performance through highly porous skeleton without compromising the electron collection. The TiO_2 on the inverse opal nanocrystal was able to achieve photocurrent density

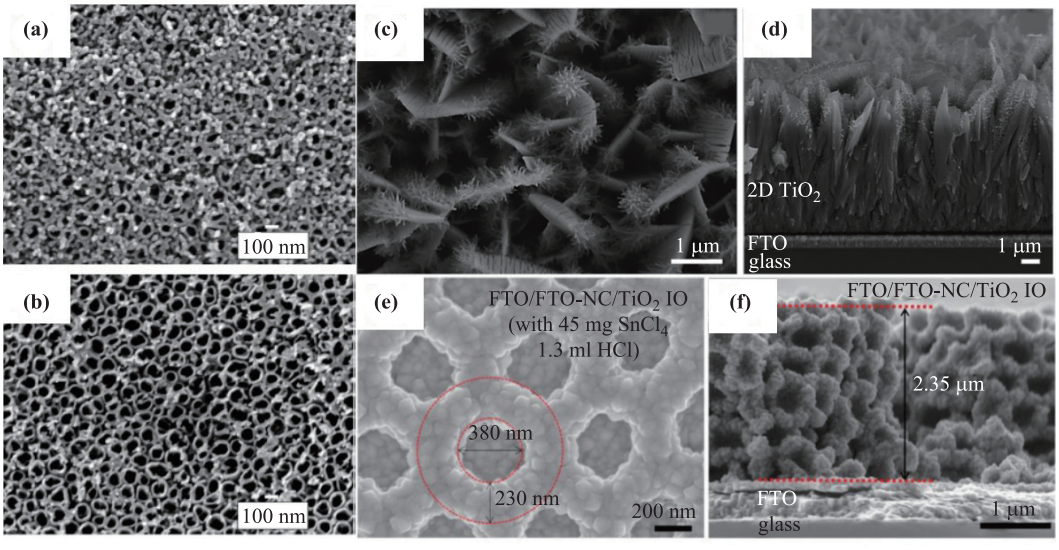

Fig. 3 Different TiO_2 morphology through nanostructuring: **(a, b)** Anodized TiO_2 nanotube. Reprinted with permission from Ref. [22]. **(c, d)** 2D anatase TiO_2 porous single-crystalline nanostructure (PSNs). Reproduced with permission from Ref. [18]. **(e, f)** 3D FTO inverse opal nanocrystal as conductive host for atomic layer deposited TiO_2. Reproduced with permission from Ref. [19].

of 1.0 mA·cm^{-2} at 1.23 V_{RHE}.

Due to the wide bandgap nature, TiO_2 is often coupled with another semiconductor with smaller bandgap to improve the amount of solar energy being harvested by the photoelectrode. Liu *et al.* deposited bismuth vanadate ($BiVO_4$), an n-type semiconductor with bandgap ~2.4 eV, onto inverse opal nanostructured TiO_2 to enable the photoelectrode to absorb wider range of solar spectrum [20]. The band structure of these two semiconductors also allow the formation of the favorable type 2 heterojunction, which can enhance the charge separation within the semiconductor. Further, they used photo-assisted electrodeposition to deposit cobalt-phosphate (Co-Pi) on $BiVO_4$ that leads to 9.0 times photo-to-energy conversion efficiency improvement over TiO_2 inverse opal. Another work created a hierarchical Fe_2O_3 (bandgap ~2.2 eV) nanorods with TiO_2 nanosheets to enhance visible light absorption [24].

Introducing foreign elements is another popular strategy to improve the performance of TiO_2 through improving the visible light absorption and charge carrier mobility. Many elements have been used as dopant in TiO_2 photoanode, including but not limited to Fe, Rh, Co, Ni, and Si for cations; N, C, S, and B for anions [25–27]. However, recent interests have been attracted by doping TiO_2 with two different elements due to their advantages over monodoped TiO_2 in higher photocatalytic activity and visible light absorption capability. The C/N codoped TiO_2 NW as reported by Song *et al.*, was able to achieve a 253-fold improvement in visible light photoactivity when compared to bare TiO_2 NW, which is among the best reported PEC efficiencies under visible irradiation. The synergistic effect of the codopants was to improve visible light absorption capability and charge separation and transference efficiencies.

4.1.2 α-Fe_2O_3 photoanode

Hematite (α-Fe_2O_3) for solar water splitting has been researched extensively since Hardee and Bard discovered its PEC property in 1976 [28]. Hematite has many attractive properties as a promising photoelectrochemical solar water splitting material, in particular it has a bandgap of 1.9 eV to 2.2 eV that can harvest majority of the visible solar spectrum, which corresponds to a maximum photocurrent density of 12.6 mA·cm^{-2} [11]. It has a conduction band that is more positive than the HER potential of water therefore a potential bias is needed to drive the reaction [29, 30]. It is stable in neutral and alkaline aqueous solution under photocorrosion. Iron is an abundant element in the earth crust and iron oxide is an environmentally friendly material. These characteristics of hematite make it an extremely promising material for solar water splitting. However, its performance still falls behind expectation due to bulk and surface charge recombinations [31], short hole diffusion length (2–4 nm) [32], high overpotential for measurable photocurrent [11], long photon absorption depth [33, 34], and improper flat band position (0.4 V_{RHE}).

To address these challenges, approaches such as nanostructuring the hematite photoanode into nanotubes [35], nanowire [36], or nanoflakes [37], applying cocatalyst layer, and introducing foreign atom have been taken. Typically, combinations of these approaches are required to yield higher PEC performance. Most notably, Gratzel and co-workers reported a Si-doped cauliflower-like hematite modified with IrO_2 cocatalyst to achieve a photocurrent density of 3.75 mA·cm^{-2} [38]. This PEC performance from hematite was a benchmark for some time until a record photocurrent density of 4.32 mA·cm^{-2} was reported on a wormlike hematite modified with Pt and Co-Pi [39].

In recent years, layered double hydroxide (LDH) type cocatalysts have been popular due to their high OER catalytic activities. Huang *et al.* deposited NiFe LDH on Mn-doped hematite photoanode for solar water splitting [40]. Mn doping improved charge separation efficiency, while NiFe LDH shifts the onset potential negatively and enhances the charge injection efficiency to 90% at high potentials. The influence of the thickness of the coating was investigated. It was found that although thicker NiFe LDH improves light absorbance, the PEC performance is lower compared to thin overlayer. This is because thick NiFe LDH affects the light absorption on hematite. IPCE of the optimum photoanode was 25% at 350 nm wavelength incident light and 1.23 V_{RHE}. LDH type cocatalysts were also used in other works, such as NiFeAl LDH [41], ZnCo LDH [42], and NiFe LDH [35]. In another work, dual cocatalyst layers were used. Wang *et al.* fabricated $Ni(OH)_2/IrO_2$ cocatalyst coated on Ti-doped Fe_2O_3 photoanode [43]. The synergetic effect of the cocatalyst was investigated. Based on CV test and transient photocurrent test, $Ni(OH)_2$ cocatalyst was shown to be able to store charges (holes) from the photoanode, which has been widely reported [44]. IrO_2 on $Ni(OH)_2$ is said to further improve the OER efficiency. IrO_2 cocatalyst alone does not improve the charge injection efficiency much while $Ni(OH)_2$ alone improve the charge injection efficiency a little at low applied potential. However, with both catalysts loaded, the PEC performance was significantly improved. Significant increase in photovoltage can be observed with $Ni(OH)_2$ loading, leading to negative shift of the onset potential. The optimum photoanode has an IPCE of ~34% at 350 nm wavelength incident light at 1.23 V_{RHE}. Wang *et al.* synthesized 1D hematite nanoflakes with the modification of Pt and FeOOH ($FeOOH/Fe_2O_3$ NFs/Pt) through a single step immersion of hematite nanoflakes in 5 mM H_2PtCl_6 solution. Interestingly, the Pt nanolayer grew only on the iron foil, while the ultrathin FeOOH nanolayer form on the surface of hematite nanoflakes [see Fig. 4(e)]. This selectively integrated hole-transfer layer (FeOOH) and electron collector layer (Pt) into hematite nanoflakes photoanode can reduce the charge recombination at the interface, which improved photocurrent density at low applied bias

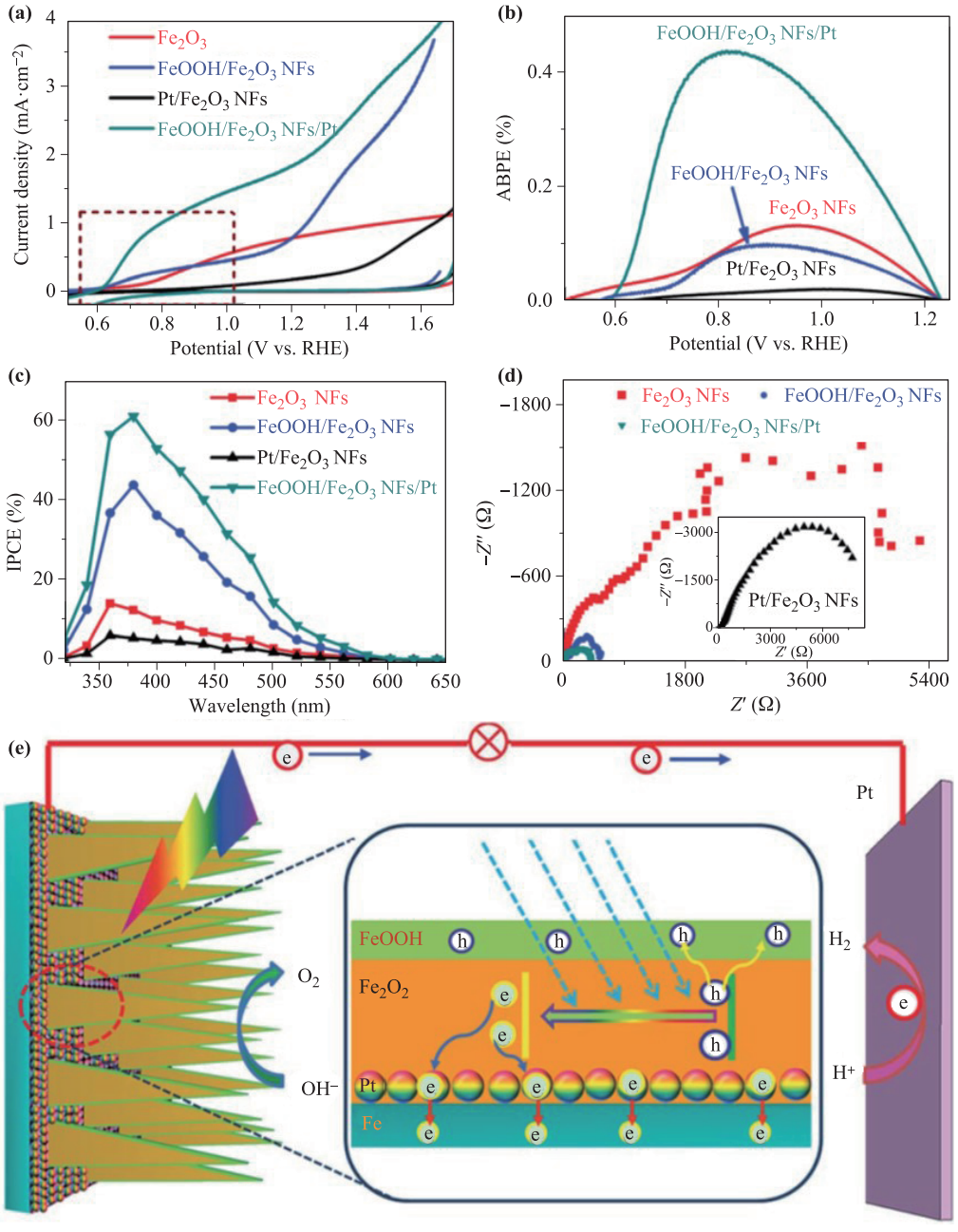

Fig. 4 **(a)** Photocurrent density vs. potential (J–V) curves of different samples. **(b)** Applied bias photo-to-current efficiency (ABPE) curves of different samples. **(c)** IPCE measurements of different samples. **(d)** Electrochemical impedance spectroscopy (EIS) measurements of different samples. **(e)** Schematic illustration of charge separation and transfer on FeOOH/Fe_2O_3 NFs/Pt. Reproduced with permission from Ref. [45].

[shown in Fig. 4(a)]. IPCE has been drastically improved and the Nyquist plot measurement indicated the reduction of charge transfer resistance upon the modification [see Figs. 4(c) and (d)].

The effect of different dopants has on the function of cocatalyst layer plays on the hematite photoanode was investigated by Tsygonok [46]. It was found that with Sn doping, $Fe_{1-x}Ni_xOOH$ cocatalyst improves the PEC performance by reducing the recombination current. On the other hand, for Zn-doped hematite, $Fe_{1-x}Ni_xOOH$ cocatalyst not only reduces recombination current, but also improves hole current. This study suggested a possible link between the surface and bulk PEC processes.

4.1.3 $BiVO_4$ photoanode

Bismuth Vanadate ($BiVO_4$) is another promising n-type semiconductor material with a bandgap slightly larger than hematite at 2.4 eV, comprises of nontoxic, low cost material with good stability. The valence band edge of

bismuth vanadate is approximately at 2.4 eV_{RHE} which means it has a conduction band minimum closed to 0 eV (0.02 eV_{RHE}) [47], hydrogen reduction potential at standard condition, the onset potential for photoelectrochemical measurement should be closed to 0 V_{RHE}. Under standard AM 1.5 G solar illumination, the theoretical STH efficiency of this material is 9.2%, an efficiency closed to the commercialized requirement for solar water splitting [48]. Despite the beneficial characteristics, $BiVO_4$ suffers from some drawbacks that lead to its low performance. Major challenges of $BiVO_4$ are: i) Poor OER kinetics, which results in surface recombination. ii) Short minority carrier diffusion length, ~70 nm. iii) Less than optimal CB edge position which requires an external bias to drive the thermodynamics of water splitting.

To overcome the aforementioned challenges, a combination of photoelectrode design strategies are often used. Lv *et al.* fabricated $BiVO_4$ porous photoanodes modified with carbon dots (CD) and NiFe-LDH to enable efficient solar water splitting [49]. The improvement of PEC performance is mainly attributed to the catalytic ability arises from the synergetic effect between CD and NiFe-LDH. The photocurrent density improved from 0.79 $mA{\cdot}cm^{-2}$ for the bare $BiVO_4$ to 2.84 $mA{\cdot}cm^{-2}$ for CDs/NiFe-LDH/$BiVO_4$. The IPCE values improved from 19.17% to 40.94% at 380 nm at 1.23 V_{RHE}. In another work, Xu *et al.* modified $BiVO_4$ photoanode by two cocatalysts, AgO_x and NiO_x, to improve the charge injection efficiency and the bulk charge separation efficiency [50]. EIS showed significant reduction of surface charge transfer resistance of the $BiVO_4/AgO_x/NiO_x$ sample at the interface with electrolyte. The use of photoassisted kelvin probe force microscopy (KPFM) showed that the final sample has higher surface photovoltage (SPV) compared to other samples that can facilitate large band bending for efficient bulk charge separation. IPCE was measured to be ~49.3% in the range of 380-450 nm wavelength at 1.23 V_{RHE} [see Figs. 5(a)–(d)]. Schematic illustration of the photoelectrode design and solar water splitting mechanism is shown in Fig. 5(e).

Prusian blue type catalysts have also been used recently, as they are cheap, environmentally friendly, highly stable, and easy to synthesize [51, 52]. Recently, Shaddad *et al.* fabricated Zr-doped $BiVO_4$/Nickel Iron Prussian blue (NiFePB) core shell photoanode [53], which were found to have improved charge transfer and charge separation efficiency over bare Zr-doped $BiVO_4$. EIS test showed a decrease in charge transfer resistance, especially at low potential. Bandgap was shown to decrease with the deposition of the NiFePB. High stability was achieved for a 50 h stability test under simulated solar irradiation.

Tandem cell with two semiconductors forming a heterogeneous junction can be helpful in facilitating charge transport within the semiconductors. For instance, Kim and Choi constructed a heterojunction of $BiVO_4/ZnFe_2O_4$ that was able to achieve ~2 $mA{\cdot}cm^{-2}$ at 1.23 V_{RHE} [54]. The $ZnFe_2O_4$ layer also improved the stability of $BiVO_4$ photoanode. The design of two heterojunctions has also been reported. $BiVO_4/WO_3/SnO_2$ photoanode was able to achieved ~3.1 $mA{\cdot}cm^{-2}$ at 1.23 V_{RHE} with IPCE value at ~70% at 300 nm wavelength light at 1.23 V_{RHE} [55]. In another work, McDowell deposited TiO_2 and Ni thin layer onto $BiVO_4$ to achieve stable photocurrent over a duration of 4 hours [56].

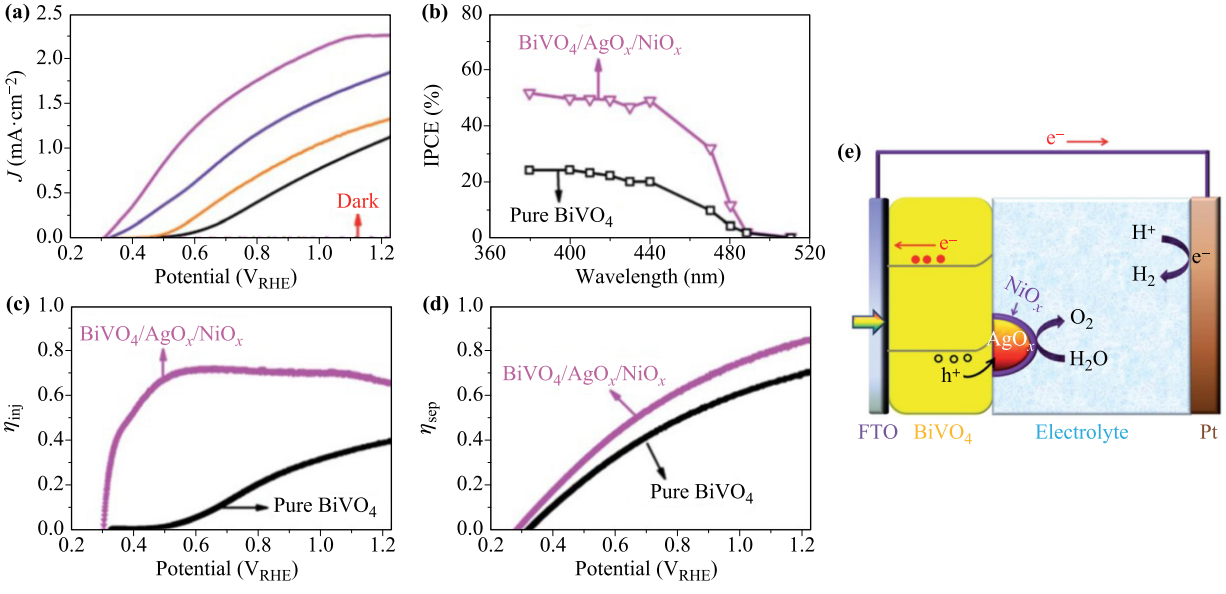

Fig. 5 **(a)** *J–V* curves with $BiVO_4/AgO_x$ (orange), BiVO4/NiO_x (violet). **(b)** IPCE curves. **(c)** Charge injection efficiency. **(d)** Charge separation efficiency. **(e)** Schematic of solar water splitting mechanisms on $BiVO_4/AgO_x/NiO_x$. Reproduced with permission from Ref. [50].

4.2 Photocathode

4.2.1 p-NiO photocathode

p-NiO is a p-type semiconductor with reported bandgap ranging from 3.3 eV [57] to 4.3 eV [58]. The Fermi level is ~0.5 eV_{RHE} (at pH 0) with valence band maximum (VBM) at ~0.4 eV more positive than the Fermi level (i.e., VBM is ~0.9 eV_{RHE}) [58–61]. NiO is an insulator at room temperature [62]. However, its conductivity can be improved by increasing the concentration of Ni^{3+} through lithium doping, nickel vacancies, or interstitial oxygen in p-NiO crystallites [63–65]. The wide bandgap of p-NiO semiconductor limits its ability to utilize wider solar spectrum, thus limit the maximum photocurrent density that can be generated from the semiconductor. As a result, there are relatively limited works on using p-NiO for PEC water splitting.

In an effort of nanostructuring the p-NiO photocathode, nickel foil was first anodized under different applied voltages and subsequently annealed under different temperature to get the desirable porosity and surface properties [66–68]. Commonly, the morphology results from anodization is nanotubes for other metals, however, macroporous structure was obtained for NiO due to rapid dissolution of the oxidized product. Hu *et al.* reported using anodized p-NiO microporous structure for PEC water splitting. Al_2O_3 was used to modify the surface of NiO to suppress the back recombination between photogenerated electron–hole pairs and stabilize the p-NiO photocathode. Sapi *et al.* used Pt nanoparticles as cocatalyst to further improve the p-NiO film. The changes in charge transfer efficiency and porosity upon the Pt nanoparticles loadings were investigated [68]. Flake-like nanostructured p-NiO can be obtained through a hydrothermal method [69]. WO_3 photoanode with smaller bandgap (~2.26 eV) was deposited on the p-NiO nanoflake to widen illumination absorption range. The p–n junction can facilitate separation of photo-generated electron–hole pairs, thus improved the photocurrent density by 3.94 times compared to p-NiO nanoflake.

Introducing a lower bandgap semiconductor to p-NiO can widen the absorption range on solar energy spectrum. Suzuki *et al.* deposited CdS (bandgap ~2.3 eV) nanoparticles on p-NiO as photosensitizer, which greatly enhanced the visible light absorption [67]. In another work, CdSe (bandgap ~1.74 eV) was used as photosensitizer for p-NiO [70]. Introducing organic dye onto p-NiO photocathode has been a popular practice in dye sensitize solar cell research [71]. There are a few works that utilized dye sensitized p-NiO in PEC hydrogen generation. Excitation of a dye molecule by solar energy can promote an electron from the highest occupied molecular orbital (HOMO) to the lowest unoccupied molecular level (LUMO). In this case, the HOMO-LUMO gap of a dye molecule is analogous to the band gap of a semiconductor. Unlike dye-sensitized photoanodes, dye-sensitized NiO photocathodes have shown to be stable under alkaline and neutral aqueous environment for HER [72, 73]. Tong *et al.* achieved stable HER with a monolayer of PMI-6T-TPA donor-acceptor type dye deposited on p-NiO photocathode [Fig. 6(a)]. The incorporation of dye improved visible light absorption of p-NiO and facilitated charge transfer from the photocathode to the electrolyte [Fig. 6(b)]. A schematic diagram of the dye-sensitized p-NiO is shown in Fig. 6(c). Some researchers even demonstrated its stability under acidic solution [74]. More detailed and comprehensive review on dye sensitized photocathode has been conducted previously [74].

5 Photoelectrochemical (PEC) CO_2 reduction systems

Generally, the PEC cell for CO_2 reduction consists of a semiconductor photocathode and a counter anode (Fig. 7). The photocathode absorbs light to produce electron–hole for catalytic reactions. The light utilization efficiency, including the absorption of incident photons, charge separation and migration, is pivotal for the performance of the PEC cell. However, PEC CO_2 reduction system usually suffers from weak light harvesting, serious charge recombination and slow electron migration rate at photocathodes [75]. Engineering the nanostructure or electronic properties of photocathode has been shown as effective methods to overcome the above drawbacks. In this section, we will mainly summarize the popular designs of photocathodes for improving the efficiency of CO_2 reduction.

5.1 Introduction of hetero-dopants

Introduction of dopant is an effective way for modifying the electronic properties of semiconductor and tuning the light harvesting efficiency [77]. The dopants can alter the type of semiconductor. A representative example is that the doped silicon [78]. Introducing the N or P element into silicon results in n-type properties, while B or Ga element results in p-type properties. In addition, dopant introduction can alter the CB or VB position of semiconductor. Non-metal dopant usually affects the CB edge but hybridizes VB to shift it upward, and thus narrows the band gap [79]. However, metal-based dopants can induce the formation of impurity in forbidden band and then increase the charge transfer ability by serving as either an electron donor or an acceptor. The band gap can be narrowed or splitted into a two-step excitation process by introducing impurity, leading to an obvious redshift of light absorption [80]. For example, the carrier density in Nb-doped TiO_2 nanowires was up to ~10^{21} cm^{-3}, which is a dramatic improvement compared to the original sample [81]. In addition, the metal dopants can also act as active centers for catalysis reactions. Such as the Cu-doped TiO_2, which

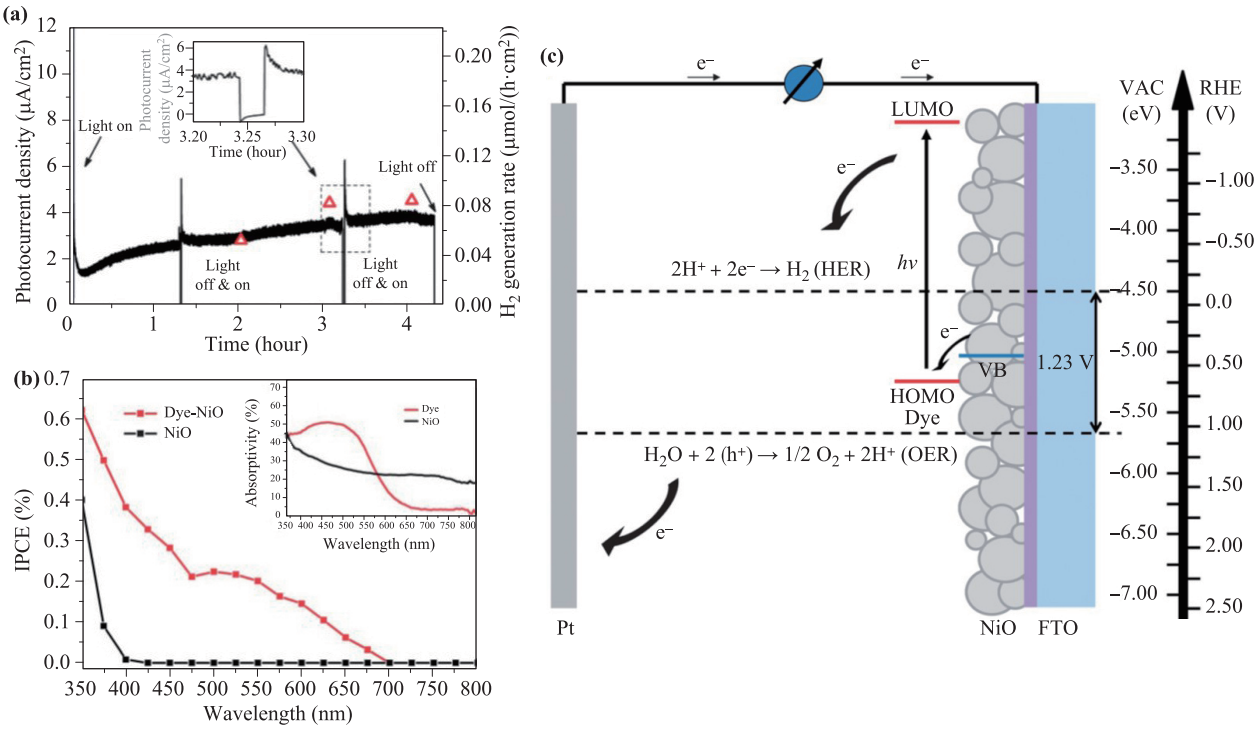

Fig. 6 **(a)** Chronoamperogram (left axis) and hydrogen generation rate (right axis, red triangles) of dye-sensitized p-NiO. **(b)** IPCE (%) spectrum and absorptivity (inset) UV-Vis absorbance of p-NiO and dye-sensitized p-NiO. **(c)** Schematic of charge transfer for HER on the dye-sensitized p-NiO photocathode. Reproduced with permission from Ref. [73].

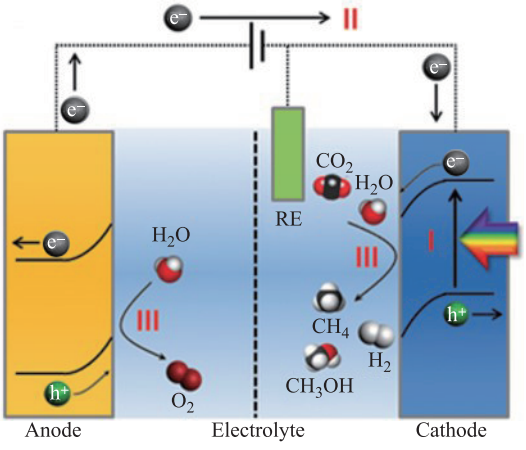

Fig. 7 Schematic of PEC CO_2 electrolyzer with a photocathode for CO_2 reduction, a photoanode for OER, and a reference electrode. Reproduced with permission from Ref. [76].

shows good selectivity in PEC CO_2 conversion to CH_3OH [82]. Li *et al.* reported the N-doped CuO with more negative CB and lower overpotential for high efficiency PEC conversion of CO_2 to methanol [83]. The carrier concentration of N-doped CuO reaches 7.5×10^{11} cm^{-3}, which is about 10^8 times of that in pristine CuO film. In 2016, Ohno *et al.* incorporated boron into graphitic carbon nitride (g-C_3N_4) and realized a 5-time improvement of the PEC current compared to the pure g-C_3N_4 [84].

Despite the doping strategy has been widely investigated on the design of photocathodes, its development for PEC CO_2 reduction is still in infant stage. We expect that more types of dopants can be discovered for constructing novel photocathodes and improving the efficiency of PEC CO_2 reduction system.

5.2 One-dimensional nanostructures

Benefiting from the unique morphology and electronic characteristics, one-dimensional (1D) nanostructures have been widely used in high-performance PEC water splitting and shows immense potentials in PEC CO_2 reduction [85, 86]. For 1D nanomaterials, the electronic wavefunction is confined within the nanoscale directions, which leads to the quantum confinement effect and then benefits the light utilization [87]. Moreover, its high length-to-diameter ratio can improve light absorption and shorten the length of electron migration, which finally results in high photon-to-electron conversion efficiency [88].

In recent, some 1D semiconductor-based photocathode have been reported for PEC CO_2 reduction. Taking the 1D p-Si as an example, the faradaic efficiency was doubled with 1D p-Si photocathode, compared to the planar counterpart [89]. Another typical case is the construction of Cu-ZnO/GaN/n^+-p Si photocathode into nanowire arrays [Figs. 8(a) and (b)] [90], which realized the tunable syngas (CO/H_2) production from CO_2 and H_2O with a 70% faradic efficiency for CO at overpotential of 180 mV. In

2016, Yang *et al.* utilized the semiconductor Si nanowires as the substrate and directly assembled Au_3Cu nanoparticle on its surface for PEC CO_2 reduction [Figs. 8(c) and (d)] [91]. This rationally designed photocathode showed a high CO_2-to-CO selectivity of ~80% at −0.20 V_{RHE} with suppressed HER. The enhancement could be partially ascribed to the superior light trapping and efficient charge transfer induced by the 1D structure. The 1D structure favors photon harvesting and exposes more active sites, exhibiting high selectivity and faradaic efficiency for PEC CO_2 conversion. Similar improvements toward PEC CO_2 reduction have been achieved on other 1D nanostructures based on p-type metal oxides, such as Cu_2O [92, 93] and Co_3O_4 [94], etc.

5.3 Construction of heterojunctions

It is difficult to simultaneously optimize the three processes of light harvesting, charge separation and migration, and redox reaction in a single material owing to the thermodynamic limitation in PEC systems. However, the barriers could be overcome by integrating semiconductors with Schottky junctions. The Schottky junction can promote the migration of charge carriers (i.e., electrons for p-type semiconductors), and then increase the separation and utilization of the electrons [95]. For example, Lee *et al.* reported that the Schottky junction by anchoring Au cocatalyst, which has smaller work function of 5.1-5.3 eV, on ZnTe (5.79 eV) can significantly improve the conversion efficiency of the ZnTe photocathode. This is because the Schottky junction (Au/ZnTe) enhanced the band bending of ZnTe and then promoted the migration of electrons from the bulk to Au, and finally transferred them to the electron acceptor in electrolyte. Moreover, the surface Au cocatalyst can provide reaction sites to CO_2 reduction by suppressing the undesired hydrogen evolution reaction [96]. Recently, Atwater *et al.* reported an Au/p-GaN Schottky junction by loading the Au nanoparticles on p-GaN photocathode, which promoted the transfer of photogenerated electrons from the p-GaN to Au and the hot holes in the opposite direction [Figs. 9(a) and (b)] [97].

Besides ZnTe, Cu_2O is also a promising semiconductor for PEC CO_2 reduction. The high-efficiency charge-separation effect of the Schottky junction between Au-Cu nanoalloys and a 3D graphene/Cu_2O photocathode has been demonstrated by Hou *et al.* Such a construction showed effective conversion of CO_2 to methanol in PEC system [98].

Although the p-type photocathodes are widely used in PEC system, they suffer from relatively low stability in aqueous solutions [100]. Coating the photocathode with a heterojunction layer has been demonstrated as an effective approach to improve its corrosion resistance. In this design, the minimal band offset and high-quality interface are needed for facilitating charge transport and suppressing recombination respectively [101]. Silicide [102], TiO_2 [103] and $SrTiO_3$ [104] have been demonstrated as protective layers in PEC CO_2 reduction. For example, as shown

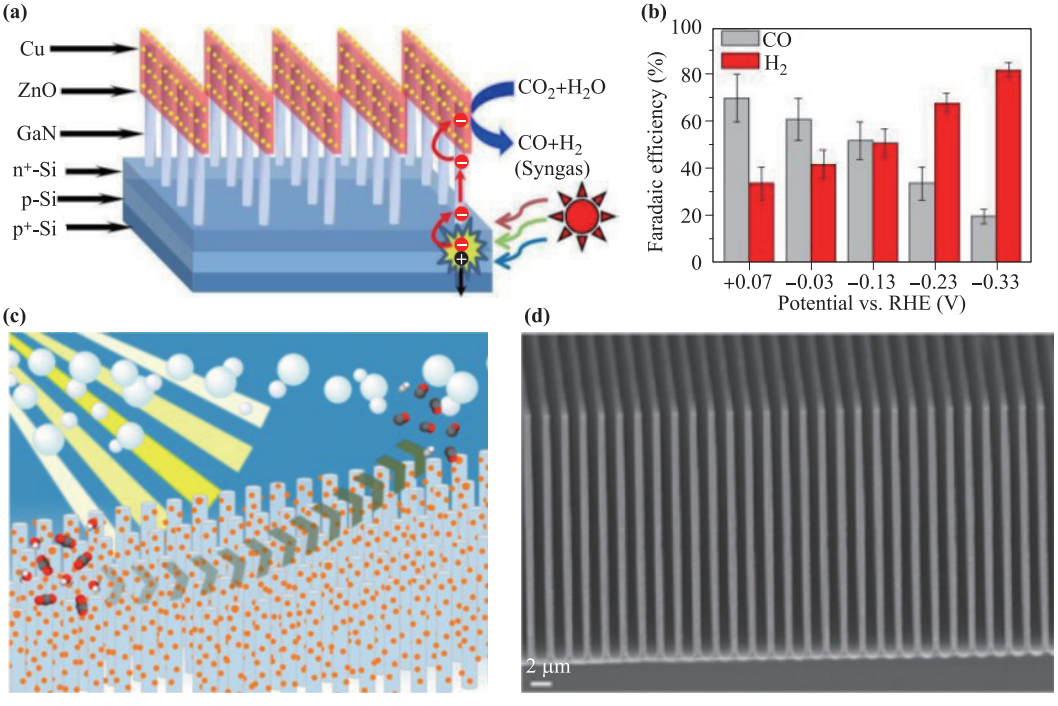

Fig. 8 **(a)** Schematic of 1D Cu-ZnO/GaN/n^+-p Si photocathode. **(b)** Faradaic efficiencies of CO and H_2 on 1D Cu-ZnO/GaN/n^+-p Si photocathode in 0.5 M $KHCO_3$ electrolyte. Reproduced with permission from Ref. [90]. **(c, d)** Schematic and SEM image of the 1D SI nanowires with Au_3Cu nanoparticle cocatalyst. Reproduced with permission from Ref. [91].

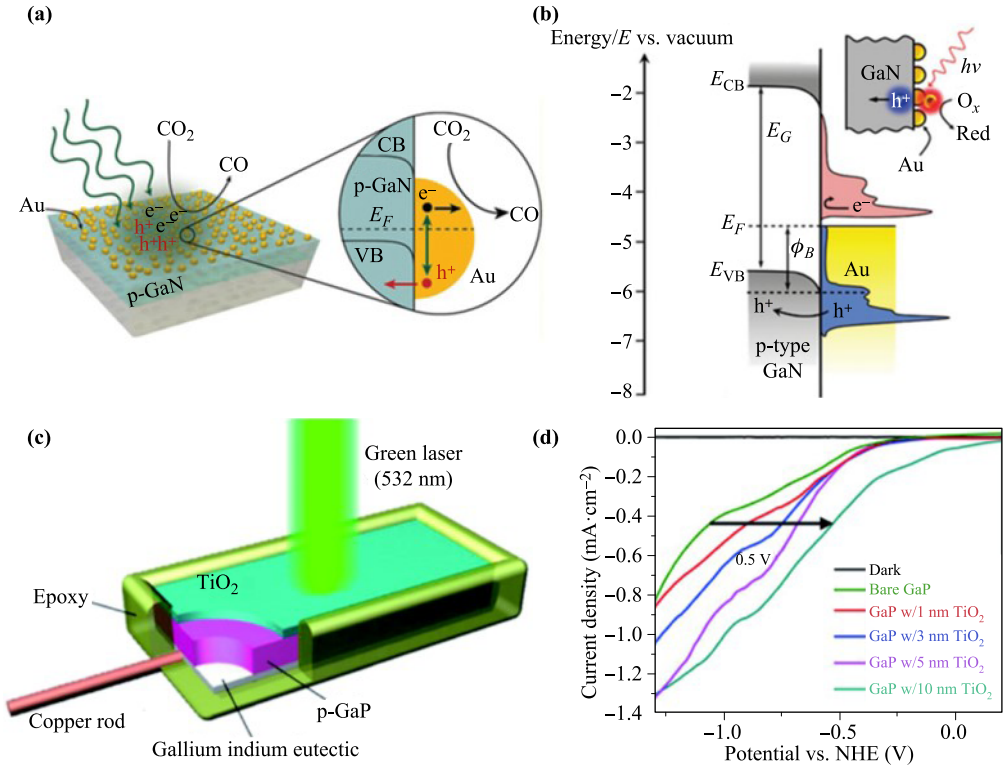

Fig. 9 **(a)** Schematic illustration of Au nanoparticle as cocatalyst anchored on p-GaN photocathode for PEC reduction of CO_2 to CO. **(b)** Energy band scheme of a plasmonic Au metal in contact with p-GaN and the corresponding Schottky junction. Reproduced with permission from Ref. [97]. **(c)** Schematic for the p-GaP photocathode passivated by TiO_2 layer. **(d)** Photocatalytic plots of p-GaP photocathodes coated TiO_2 layer at various thicknesses. Reproduced with permission from Ref. [99].

in Fig. 9(c), a n-type TiO_2 layer with a thickness of 10 nm was coated on p-GaP using atomic layer deposition (ALD) [99], which passivated the surface and provided a substantial enhancement on the photoconversion efficiency. Moreover, a p–n junction was formed in this construction. Benefiting from the above merits, the heterojunction photocathode showed a 0.5 V reduction in onset overpotential for CO_2 to CH_3OH [Fig. 9(d)].

5.4 Utilizations of cocatalysts on photocathodes for PEC CO_2 reduction

The efficiency of CO_2 reduction is limited by the sluggish kinetics, which leads to a large overpotential and decreases the conversion efficiency. The CO_2 adsorption and activation are the initial steps for the subsequent PEC reductions, in which the photocathodes act as both light harvesting antennas and catalytic centers. Despite huge efforts have been devoted to improving light utilization efficiency, photocathode surface shows poor adsorption and activation abilities for CO_2, leading to low conversion efficiency of CO_2 to hydrocarbon [105, 106]. Anchoring cocatalysts on semiconductor surface has been proved to be an effective approach to improve the efficiency of PEC CO_2 reduction [107–109]. The cocatalysts can lower the overpotential and reduce the energy barrier, facilitating CO_2 activation as well as improving the selectivity. In this part, we will introduce various types of cocatalysts and discuss their roles in the CO_2 reduction process.

5.4.1 *Metal-based cocatalysts*

Integrating semiconductor with metal nanoparticle cocatalysts is an effective way to improve the PEC performance [109, 110]. The metal cocatalysts can trap the photoinduced charges to promote charge separation and provide active centers to facilitate CO_2 reduction reactions. Besides, the undesired side reaction of HER can be suppressed in the PEC CO_2 reduction system with the right metal cocatalyst(s).

Some metals are competent to act as active sites for the reduction of CO_2 to CO, such as Au [111], Ag [112], and Pd [113], while some other metals such as Sn [114] and Pb [115] show good selectivity for producing formate from CO_2. Moreover, Cu can produce various hydrocarbon products when used as electrode for CO_2 reduction due to the poor selectivity. Nevertheless, Cu has received extensive attention [98, 116, 117]. Kaneco *et al.* [118] anchored the Pb, Ag, Au, Pd, Cu, and Ni on p-InP semiconductor for PEC CO_2 reduction, and reported that the Pb, Ag, Au and Cu can produce both CO and HCOOH

and Pd shows good selectivity for CO. By summarizing the previous reported literature, it can be concluded that anchoring metal nanoparticles on photocathode can positively shift the overpotential of CO_2 reduction and control the selectivity of products. For instance, by modifying the p-Si photocathode with Cu, Ag, and Au for PEC CO_2 reduction, the overpotential was positively shifted and the major products also changed from CO and HCOOH to CH_4 and C_2H_4 [119].

Besides the noble metal cocatalysts described above, several earth-abundant metals have been demonstrated as effective cocatalysts for PEC CO_2 reduction, such as Co [123], Ni [124], Mn [125], and Fe [126]. For example, a highly active Fe porphyrin complex was grafted on B-doped p-Si photocathode for CO_2 reduction [127], which exhibited a significant improvement for CO evolution with faradaic efficiency of 80% after 6 h of reaction by effectively suppressing HER. As shown in Fig. 10(a), a molecular manganese catalyst (*fac*-[MnBr(4, 4′-*bis*(phosphonicacid)-2, 2′-bipyridine) $(CO)_3$]) was integrated with the TiO_2 electrode to achieve a 67.5% faradaic efficiency during the PEC CO_2-to-CO reduction [120]. Moreover, this work revealed the dynamic reconstruction of the Mn-Mn dimer active site on the TiO_2 electrode surface. Despite the metal complex-based cocatalysts have shown promising performance in PEC CO_2 conversion, the products mainly focus on two-electron reduction products like CO and HCOOH and higher-value hydrocarbon products (such as CH_3OH and CH_4) are rarely reported. Very recently, a trimethylammonio functionalized iron tetraphenylporphyrin complex was reported to produce eight-electron reduction product of CH_4 by integrating with Ir-based light sensitizer [128]. In which the CO was initially achieved and then converted into CH_4 with an impressive selectivity of ~82%. Therefore, the metal complex-based cocatalyst for PEC CO_2 reduction can be further developed to produce higher-value hydrocarbons with better efficiency.

5.4.2 Metal-free cocatalysts

Besides the metal-based cocatalysts, the metal-free cocatalysts like organic molecules and polymers have also shown promising performances for PEC CO_2 reduction. An representative example is the dissolved tetraalkylammonium (NR^{4+}, R = hydrocarbyl) salts on photocathodes, which can improve the activity and modulate the selectivity during PEC CO_2 reduction [129, 130]. This is because the NR^{4+} species in electrolyte can adsorb on photocathodes and block the adsorption of H_2O and then hinder the competing HER process. Moreover, the NR^{4+} ions can capture electrons from photocathode and then promote the activation of CO_2 into -CO_2 by forming NR_4 radical intermediates.

The conductive polymers such as polypyrrole and polycation have been proven as effective cocatalysts for improving PEC CO_2 reduction, because the rich functional

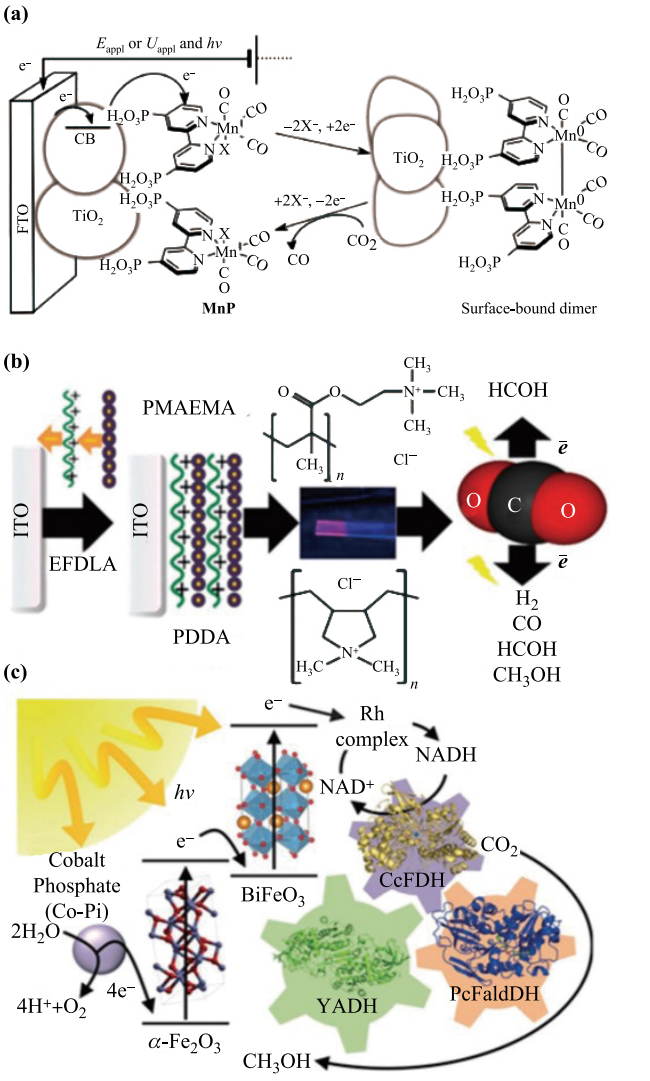

Fig. 10 **(a)** Schematic of molecular Mn cocatalyst on mesoporous TiO_2 for PEC CO_2 reduction. Reproduced with permission from Ref. [120]. **(b)** Schematic illustrations of PDDA/CdTe QDs or PMAEMA/CdTe QDs for PEC CO_2 reduction. Reprinted with permission from Ref. [121]. **(c)** A tandem PEC enzyme-cascade electrolyzer including the Rh complex and three dehydrogenases for PEC CO_2 conversion to CH_3OH. Reproduced with permission from Ref. [122].

groups in polymers can promote the CO_2 reduction selectivity by binding with reaction molecules and modulating the adsorption of reaction intermediates [121, 131]. For instance, Isaacs *et al.* explored the behaviors of poly-diallyldimethylammonium (PDDA) and poly(2-trimethylammonium)ethyl methacrylate (PMAEMA) in PEC CO_2 reduction system by combining with CdTe quantum dots (QDs) via an electric field directed layer-by-layer assembly (EFDLA) method [Fig. 10(b)] [121]. The CO_2 reduction activity is related to the structure of the polycation and its assembly with QDs. Moreover, the distribution of reduction products is also associated with

the polycation type. Specifically, the PDDA/QDs assembly lead to the formation of CO, HCHO, and CH_3OH but PMAEMA/QDs assembly trigger the conversion to HCHO.

5.4.3 Biological cocatalysts

Recently, many works have reported the developments on natural enzymes as promising cocatalysts for PEC CO_2 reduction [122, 132, 133]. The loading of biological cocatalysts onto semiconductors can provide highly active centers for PEC CO_2 reduction, leading to high performance and good selectivity for hydrocarbon products. For example, Park *et al.* constructed a tandem PEC electrolyzer by integrating enzyme-cascade (TPIEC), which can transfer photo-induced electrons to a multienzyme cascade for the conversion of CO_2 to methanol. In that reaction system, the nicotinamide cofactor (NADH) was consumed by dehydrogenases to produce NAD^+, and then the NAD^+ was reduced to NADH. Under external bias, this TPIEC system exhibited an impressive CO_2-to-methanol conversion rate of 1280 $\mu mol \cdot g^{-1} \cdot h^{-1}$ [Fig. 10(c)] [122]. Armstrong and co-workers also developed a carbon monoxide dehydrogenase (CODH) from carboxydothermus hydrogenoformans as a cocatalyst for a dye-sensitized p-NiO semiconductor and used it in PEC CO_2 reduction, which showed good selectively to reduce CO_2 into CO under visible-light [132, 133].

6 Conclusions and prospects

Recent progresses on the design of photoelectrode for PEC water splitting and CO_2 reduction are summarized and discussed in this review article. In the context of PEC water splitting, many research efforts have been focused on enabling more visible light utilization by the transition metal oxide semiconductors through nanostructuring and energy band engineering. However, the achievement of high photocurrent density often involves the use of noble metals. A few potential directions for future research could be:

(1) PEC water splitting cell under neutral or close to neutral conditions. Most existing PEC cells use acidic or basic solution, which pose potential hazards especially when leakage occurs.

(2) The use of noble metal in photoelectrode design can provide mechanistic understanding of the underlying photoelectrochemistry processes. However, in view of the end goal of deploying the PEC water splitting cell, cheap and earth abundant cocatalyst should be the focus.

(3) Although only a few common transition metal oxide semiconductors are reviewed in this article, new and emerging materials should be explored and investigated with the knowledge built upon these well-studied semiconductor materials.

In the context of PEC CO_2 reduction, despite a series of exciting progresses have been achieved, our understanding of the PEC CO_2 reduction process remains limited. There are still many challenges:

(1) In the currently widely used cocatalysts for PEC CO_2 reduction system, most of the catalyst are based on the high-cost and scarce noble metals. Developing alternative cocatalysts that are based on earth-abundant and low-cost elements are imperative. To date, the Cu-based catalysts show promising effects in PEC CO_2 reduction, but they have low selectivity and usually produce a wide distribution of products. Therefore, improving the selectivity of Cu-based catalysts is of great significance.

(2) Improving PEC conversion efficiency of solar energy to CO_2 is necessary. High-efficiency of light utilization is important in increasing CO_2 reduction yield.

(3) The fundamental but complicated mechanism in PEC CO_2 reduction on a photocathode need to be further investigated, such as identifying the catalytic sites and reaction intermediates, which will better guide the development of highly effective catalysts.

Contributions Y. H. L. and B. Z. mainly worked on the solar water splitting part and solar CO_2 reduction part, respectively. All authors contributed to the writing of the manuscript.

Acknowledgements The authors would like to acknowledge the funding support from U.S. National Science Foundation (NSF-CMMI-1663509).

References

1. I. Roger, M. A. Shipman, and M. D. Symes, Earth-abundant catalysts for electrochemical and photoelectrochemical water splitting, *Nat. Rev. Chem.* 1(1), 0003 (2017)
2. T. Hisatomi and K. Domen, Introductory lecture: Sunlight-driven water splitting and carbon dioxide reduction by heterogeneous semiconductor systems as key processes in artificial photosynthesis, *Faraday Discuss.* 198, 11 (2017)
3. M. G. Walter, E. L. Warren, J. R. McKone, S. W. Boettcher, Q. Mi, E. A. Santori, and N. S. Lewis, Solar water splitting cells, *Chem. Rev.* 110(11), 6446 (2010)
4. B. Zhang, Y. H. Lui, H. Ni, and S. Hu, Bimetallic $(Fe_xNi_{1-x})_2P$ nanoarrays as exceptionally efficient electrocatalysts for oxygen evolution in alkaline and neutral media, *Nano Energy* 38, 553 (2017)
5. B. Zhang, Y. H. Lui, A. P. S. Gaur, B. Chen, X. Tang, Z. Qi, and S. Hu, Hierarchical FeNiP@ultrathin carbon nanoflakes as alkaline oxygen evolution and acidic hydrogen evolution catalyst for efficient water electrolysis and organic decomposition, *ACS Appl. Mater. Interfaces* 10(10), 8739 (2018)
6. M. Schreier, L. Curvat, F. Giordano, L. Steier, A. Abate, S. M. Zakeeruddin, J. Luo, M. T. Mayer, and M. Grätzel, Efficient photosynthesis of carbon monoxide from CO_2

using perovskite photovoltaics, *Nat. Commun.* 6(1), 7326 (2015)

7. J. Luo, J.-H. Im, M. T. Mayer, M. Schreier, M. Khaja Nazeeruddin, N.-G. Park, S. David Tilley, H. J. Fan, and M. Grätzel, Water photolysis at 12.3% efficiency via perovskite photovoltaics and Earth-abundant catalysts, *Science* 345(6204), 1593 (2014)
8. J. K. Stolarczyk, S. Bhattacharyya, L. Polavarapu, and J. Feldmann, Challenges and prospects in solar water splitting and CO_2 reduction with inorganic and hybrid nanostructures, *ACS Catal.* 8(4), 3602 (2018)
9. A. Fujishima and K. Honda, Electrochemical photolysis of water at a semiconductor electrode, *Nature* 238(5358), 37 (1972)
10. T. Inoue, A. Fujishima, S. Konishi, and K. Honda, Photoelectrocatalytic reduction of carbon dioxide in aqueous suspensions of semiconductor powders, *Nature* 277(5698), 637 (1979)
11. K. Sivula, F. Le Formal, and M. Grätzel, Solar water splitting: Progress using hematite (α-Fe_2O_3) photoelectrodes, *ChemSusChem* 4(4), 432 (2011)
12. X. Shi, L. Cai, M. Ma, X. Zheng, and J. H. Park, General characterization methods for photoelectrochemical cells for solar water splitting, *ChemSusChem* 8(19), 3192 (2015)
13. C. Ding, J. Shi, Z. Wang, and C. Li, Photoelectrocatalytic water splitting: Significance of cocatalysts, electrolyte, and interfaces, *ACS Catal.* 7(1), 675 (2017)
14. A. J. Bard and M. A. Fox, Artificial photosynthesis: Solar splitting of water to hydrogen and oxygen water splitting, *Acc. Chem. Res.* 28(3), 141 (1995)
15. X. Liu, S. Inagaki, and J. Gong, Heterogeneous molecular systems for photocatalytic CO_2 reduction with water oxidation, *Angew. Chem. Int. Ed.* 55(48), 14924 (2016)
16. A. J. Nozik and R. Memming, Physical chemistry of semiconductor–liquid interfaces, *J. Phys. Chem.* 100(31), 13061 (1996)
17. R. Asahi, T. Morikawa, T. Ohwaki, K. Aoki, and Y. Taga, Visible-light photocatalysis in nitrogen-doped titanium oxides, *Science* 293, 2000 (2001)
18. T. Butburee, Y. Bai, H. Wang, H. Chen, Z. Wang, G. Liu, J. Zou, P. Khemthong, G. Q. M. Lu, and L. Wang, 2D porous TiO_2 single-crystalline nanostructure demonstrating high photo-electrochemical water splitting performance, *Adv. Mater.* 30(21), 1705666 (2018)
19. Z. Wang, X. Li, H. Ling, C. K. Tan, L. P. Yeo, A. C. Grimsdale, and A. I. Y. Tok, 3D FTO/FTO-nanocrystal/TiO_2 composite inverse opal photoanode for efficient photoelectrochemical water splitting, *Small* 14(20), 1800395 (2018)
20. Q. Liu, R. Mo, X. Li, S. Yang, J. Zhong, and H. Li, Cobalt phosphate modified 3D TiO_2/$BiVO_4$ composite inverse opals photoanode for enhanced photoelectrochemical water splitting, *Appl. Surf. Sci.* 464, 544 (2019)
21. G. K. Mor, K. Shankar, O. K. Varghese, and C. A. Grimes, Photoelectrochemical properties of titania nanotubes, *J. Mater. Res.* 19(10), 2989 (2004)
22. G. K. Mor, K. Shankar, M. Paulose, O. K. Varghese, and C. A. Grimes, Enhanced photocleavage of water using titania nanotube arrays, *Nano Lett.* 5(1), 191 (2005)
23. J. U. Kim, H. S. Han, J. Park, W. Park, J. H. Baek, J. M. Lee, H. S. Jung, and I. S. Cho, Facile and controllable surface-functionalization of TiO_2 nanotubes array for highly-efficient photoelectrochemical water-oxidation, *J. Catal.* 365, 138 (2018)
24. R. Zhang, M. Sun, G. Zhao, G. Yin, and B. Liu, Hierarchical Fe_2O_3 nanorods/TiO_2 nanosheets heterostructure: Growth mechanism, enhanced visible-light photocatalytic and photoelectrochemical performances, *Appl. Surf. Sci.* 475, 380 (2019)
25. S. Shen, J. Chen, M. Wang, X. Sheng, X. Chen, X. Feng, and S. S. Mao, Titanium dioxide nanostructures for photoelectrochemical applications, *Prog. Mater. Sci.* 98, 299 (2018)
26. X. Song, W. Li, D. He, H. Wu, Z. Ke, C. Jiang, G. Wang, and X. Xiao, The "Midas Touch" transformation of TiO_2 nanowire arrays during visible light photoelectrochemical performance by carbon/nitrogen coimplantation, *Adv. Energy Mater.* 8(20), 1800165 (2018)
27. Z. Dong, D. Ding, T. Li, and C. Ning, Ni-doped TiO_2 nanotubes photoanode for enhanced photoelectrochemical water splitting, *Appl. Surf. Sci.* 443, 321 (2018)
28. K. L. Hardee and A. Bard, The application of chemically vapor deposied iron oxide films to photosensitized electrolysis, *J. Electrochem. Soc.* 127, 1026 (1976)
29. K. Gelderman, L. Lee, and S. W. Donne, Flat–band potential of a semiconductor: Using the Mott–Schottky equation, *J. Chem. Educ.* 84(4), 685 (2007)
30. J. H. Kennedy, Flatband potentials and donor densities of polycrystalline α-Fe_2O_3 determined from mott-schottky plots, *J. Electrochem. Soc.* 125(5), 723 (1978)
31. I. S. Cho, H. S. Han, M. Logar, J. Park, and X. Zheng, Enhancing low-bias performance of hematite photoanodes for solar water splitting by simultaneous reduction of bulk, interface, and surface recombination pathways, *Adv. Energy Mater.* 6(4), 1501840 (2015)
32. J. H. Kennedy and K. W. Frese, Photooxidation of water at α-Fe_2O_3 electrodes, *J. Electrochem. Soc.* 125(5), 709 (1978)
33. I. Cesar, K. Sivula, A. Kay, R. Zboril, and M. Grätzel, Influence of feature size, film thickness, and silicon doping on the performance of nanostructured hematite photoanodes for solar water splitting, *J. Phys. Chem. C* 113(2), 772 (2009)
34. H. Jun, B. Im, J. Y. Y. Y. Y. Kim, Y.O. Im, J.W. Jang, E. S. Kim, J. Y. Kim, H. J. Kang, S. J. Hong, and J. S. Lee, Photoelectrochemical water splitting over ordered honeycomb hematite electrodes stabilized by alumina shielding, *Energy Environ. Sci.* 5(4), 6375 (2012)
35. D. H. Kim, D. M. Andoshe, Y. S. Shim, C. W. Moon, W. Sohn, S. Choi, T. L. Kim, M. Lee, H. Park, K. Hong, K. C. Kwon, J. M. Suh, J.S. Kim, J.H. Lee, and H. W. Jang, Toward high-performance hematite nanotube photoanodes: Charge-transfer engineering at heterointerfaces, *ACS Appl. Mater. Interfaces* 8(36), 23793 (2016)

36. L. Li, Y. Yu, F. Meng, Y. Tan, R. J. Hamers, and S. Jin, Facile solution synthesis of α-$FeF_3{\cdot}3H_2O$ nanowires and their conversion to α-Fe_2O_3 nanowires for photoelectrochemical application, *Nano Lett.* 12(2), 724 (2012)

37. L. Wang, Y. Yang, Y. Zhang, Q. Rui, B. Zhang, Z. Shen, and Y. Bi, One-dimensional hematite photoanodes with spatially separated Pt and FeOOH nanolayers for efficient solar water splitting, *J. Mater. Chem. A* 5(32), 17056 (2017)

38. A. Kay, I. Cesar, and M. Grätzel, New benchmark for water photooxidation by nanostructured α-Fe_2O_3 films, *J. Am. Chem. Soc.* 128(49), 15714 (2006)

39. J. Y. Kim, G. Magesh, D. H. Youn, J. W. Jang, J. Kubota, K. Domen, and J. S. Lee, Single-crystalline, wormlike hematite photoanodes for efficient solar water splitting, *Sci. Rep.* 3(1), 1 (2013)

40. J. Huang, G. Hu, Y. Ding, M. Pang, and B. Ma, Mn-doping and NiFe layered double hydroxide coating: Effective approaches to enhancing the performance of α-Fe_2O_3 in photoelectrochemical water oxidation, *J. Catal.* 340, 261 (2016)

41. G. Wang, B. Wang, C. Su, D. Li, L. Zhang, R. Chong, and Z. Chang, Enhancing and stabilizing α-Fe_2O_3 photoanode towards neutral water oxidation: Introducing a dual-functional NiCoAl layered double hydroxide overlayer, *J. Catal.* 359, 287 (2018)

42. H.-J. Ahn, A. Goswami, F. Riboni, S. Kment, A. Naldoni, S. Mohajernia, R. Zboril, and P. Schmuki, Hematite photoanode with complex nanoarchitecture providing tunable gradient doping and low onset potential for photoelectrochemical water splitting, *ChemSusChem* 11(11), 1873 (2018)

43. Z. Wang, G. Liu, C. Ding, Z. Chen, F. Zhang, J. Shi, and C. Li, Synergetic effect of conjugated $Ni(OH)_2/IrO_2$ cocatalyst on titanium-doped hematite photoanode for solar water splitting, *J. Phys. Chem. C* 119(34), 19607 (2015)

44. T. W. Kim and K.-S. Choi, Nanoporous $BiVO_4$ photoanodes with dual-layer oxygen evolution catalysts for solar water splitting, *Science* 343(6174), 990 (2014)

45. L. Wang, Y. Yang, Y. Zhang, Q. Rui, B. Zhang, Z. Shen, and Y. Bi, One-dimensional hematite photoanodes with spatially separated Pt and FeOOH nanolayers for efficient solar water splitting, *J. Mater. Chem. A* 5(32), 17056 (2017)

46. A. Tsyganok, D. Klotz, K. D. Malviya, A. Rothschild, and D. A. Grave, Different roles of $Fe_{1-x}Ni_xOOH$ cocatalyst on hematite (α-Fe_2O_3) photoanodes with different dopants, *ACS Catal.* 8(4), 2754 (2018)

47. Y. Park, K. J. Mcdonald, and K. S. Choi, Progress in bismuth vanadate photoanodes for use in solar water oxidation, *Chem. Soc. Rev.* 42(6), 2321 (2013)

48. Z. F. Huang, L. Pan, J. J. Zou, X. Zhang, and L. Wang, Nanostructured bismuth vanadate-based materials for solar-energy-driven water oxidation: A review on recent progress, *Nanoscale* 6(23), 14044 (2014)

49. X. Lv, X. Xiao, M. Cao, Y. Bu, C. Wang, M. Wang, and Y. Shen, Efficient carbon dots/NiFe-layered double hydroxide/$BiVO_4$ photoanodes for photoelectrochemical water splitting, *Appl. Surf. Sci.* 439, 1065 (2018)

50. Y. Hu, Y. Wu, J. Feng, H. Huang, C. Zhang, Q. Qian, T. Fang, J. Xu, P. Wang, Z. Li, and Z. Zou, Rational design of electrocatalysts for simultaneously promoting bulk charge separation and surface charge transfer in solar water splitting photoelectrodes, *J. Mater. Chem. A* 6(6), 2568 (2018)

51. H. T. Bui, N. K. Shrestha, S. Khadtare, C. D. Bathula, L. Giebeler, Y. Y. Noh, and S. H. Han, Anodically grown binder-free nickel hexacyanoferrate film: Toward efficient water reduction and hexacyanoferrate film based full device for overall water splitting, *ACS Appl. Mater. Interfaces* 9(21), 18015 (2017)

52. Y. Yamada, K. Oyama, R. Gates, and S. Fukuzumi, High catalytic activity of heteropolynuclear cyanide complexes containing cobalt and platinum ions: Visible-light driven water oxidation, *Angew. Chem. Int. Ed.* 54(19), 5613 (2015)

53. A. M. Al-Mayouf, P. Arunachalam, M. N. Shaddad, J. Labis, and M. Hezam, Fabrication of robust nanostructured (Zr)$BiVO_4$/nickel hexacyanoferrate core/shell photoanodes for solar water splitting, *Appl. Catal. B* 244, 863 (2018)

54. T. W. Kim, and K. S. Choi, Improving stability and photoelectrochemical performance of $BiVO_4$ photoanodes in basic media by adding a $ZnFe_2O_4$ layer, *J. Phys. Chem. Lett.* 7(3), 447 (2016)

55. J. H. Baek, B. J. Kim, G. S. Han, S. W. Hwang, D. R. Kim, I. S. Cho, and H. S. Jung, $BiVO_4/WO_3/SnO_2$ double-heterojunction photoanode with enhanced charge separation and visible-transparency for bias-free solar water-splitting with a perovskite solar cell, *ACS Appl. Mater. Interfaces* 9(2), 1479 (2017)

56. M. T. McDowell, M. F. Lichterman, J. M. Spurgeon, S. Hu, I. D. Sharp, B. S. Brunschwig, and N. S. Lewis, Improved stability of polycrystalline bismuth vanadate photoanodes by use of dual-layer thin TiO_2/Ni coatings, *J. Phys. Chem. C* 118(34), 19618 (2014)

57. K. Nakaoka, J. Ueyama, and K. Ogura, Semiconductor and electrochromic properties of electrochemically deposited nickel oxide films, *J. Electroanal. Chem.* 571(1), 93 (2004)

58. M. D. Irwin, D. B. Buchholz, A. W. Hains, R. P. H. Chang, and T. J. Marks, p-Type semiconducting nickel oxide as an efficiency-enhancing anode interfacial layer in polymer bulk-heterojunction solar cells, *Proc. Natl. Acad. Sci. USA* 105(8), 2783 (2008)

59. I. M. Chan, T. Y. Hsu, and F. C. Hong, Enhanced hole injections in organic light-emitting devices by depositing nickel oxide on indium tin oxide anode, *Appl. Phys. Lett.* 81(10), 1899 (2002)

60. M. T. Greiner, M. G. Helander, Z. B. Wang, W. M. Tang, and Z. H. Lu, Effects of processing conditions on the work function and energy-level alignment of NiO thin films, *J. Phys. Chem. C* 114(46), 19777 (2010)

61. F. P. Koffyberg and F. A. Benko, p-type NiO as a photoelectrolysis cathode, *J. Electrochem. Soc.* 128(11), 2476 (1981)

62. S. Hüfner, Electronic structure of NiO and related 3d-transition-metal compounds, *Adv. Phys.* 43(2), 183 (1994)

63. W. Guo, K. N. Hui, and K. S. Hui, High conductivity nickel oxide thin films by a facile sol–gel method, *Mater. Lett.* 92, 291 (2013)

64. L. Cattin, B. A. Reguig, A. Khelil, M. Morsli, K. Benchouk, and J. C. Bernède, Properties of NiO thin films deposited by chemical spray pyrolysis using different precursor solutions, *Appl. Surf. Sci.* 254(18), 5814 (2008)

65. K. Matsubara, S. Huang, M. Iwamoto, and W. Pan, Enhanced conductivity and gating effect of p-type Li-doped NiO nanowires, *Nanoscale* 6(2), 688 (2014)

66. C. Hu, K. Chu, Y. Zhao, and W. Y. Teoh, Efficient photoelectrochemical water splitting over anodized p-type NiO porous films, *ACS Appl. Mater. Interfaces* 6(21), 18558 (2014)

67. Y. Suzuki, Z. Xie, X. Lu, Y. W. Cheng, R. Amal, and Y. H. Ng, Cadmium sulfide Co-catalyst reveals the crystallinity impact of nickel oxide photocathode in photoelectrochemical water splitting, *Int. J. Hydrogen Energy* (2018)

68. A. Sápi, A. Varga, G. F. Samu, D. Dobó, K. L. Juhász, B. Takács, E. Varga, Á. Kukovecz, Z. Kónya, and C. Janáky, Photoelectrochemistry by design: Tailoring the nanoscale structure of Pt/NiO composites leads to enhanced photoelectrochemical hydrogen evolution performance, *J. Phys. Chem. C* 121(22), 12148 (2017)

69. P. Wu, Z. Liu, D. Chen, M. Zhou, and J. Wei, Flake-like NiO/WO_3 p–n heterojunction photocathode for photoelectrochemical water splitting, *Appl. Surf. Sci.* 440, 1101 (2018)

70. Y. Dong, Y. Chen, P. Jiang, G. Wang, X. Wu, R. Wu, and C. Zhang, Efficient and stable MoS_2/CdSe/NiO photocathode for photoelectrochemical hydrogen generation from water, *Chem. Asian J.* 10(8), 1660 (2015)

71. J. Gong, K. Sumathy, Q. Qiao, and Z. Zhou, Review on dye-sensitized solar cells (DSSCs): Advanced techniques and research trends, *Renew. Sustain. Energy Rev.* 68, 234 (2017)

72. Z. Ji, M. He, Z. Huang, U. Ozkan, and Y. Wu, Photostable p-type dye-sensitized photoelectrochemical cells for water reduction, *J. Am. Chem. Soc.* 135(32), 11696 (2013)

73. L. Tong, A. Iwase, A. Nattestad, U. Bach, M. Weidelener, G. Götz, A. Mishra, P. Bäuerle, R. Amal, G. G. Wallace, and A. J. Mozer, Sustained solar hydrogen generation using a dye-sensitised NiO photocathode/$BiVO_4$ tandem photo-electrochemical device, *Energy Environ. Sci.* 5(11), 9472 (2012)

74. E. A. Gibson, Dye-sensitized photocathodes for H_2 evolution, *Chem. Soc. Rev.* 46(20), 6194 (2017)

75. X. Li, J. Wen, J. Low, Y. Fang, and J. Yu, Design and fabrication of semiconductor photocatalyst for photocatalytic reduction of CO_2 to solar fuel, *Sci China Mater* 57(1), 70 (2014)

76. X. Chang, T. Wang, P. Yang, G. Zhang, and J. Gong, The development of cocatalysts for photoelectrochemical CO_2 reduction, *Adv. Mater.* 1804710, 1804710 (2018)

77. H. Tong, S. Ouyang, Y. Bi, N. Umezawa, M. Oshikiri, and J. Ye, Nano-photocatalytic materials: Possibilities and challenges, *Adv. Mater.* 24(2), 229 (2012)

78. K. Sun, S. Shen, Y. Liang, P. E. Burrows, S. S. Mao, and D. Wang, Enabling silicon for solar-fuel production, *Chem. Rev.* 114(17), 8662 (2014)

79. R. Asahi, Visible-light photocatalysis in nitrogen-doped titanium oxides, *Science* 293(5528), 269 (2001)

80. W. Yang, D. Chen, H. Quan, S. Wu, X. Luo, and L. Guo, Enhanced photocatalytic properties of $ZnFe_2O_4$-doped $ZnIn_2S_4$ heterostructure under visible light irradiation, *RSC Adv.* 6(86), 83012 (2016)

81. B. Liu, H. M. Chen, C. Liu, S. C. Andrews, C. Hahn, and P. Yang, Large-scale synthesis of transition-metal-doped TiO_2 nanowires with controllable overpotential, *J. Am. Chem. Soc.* 135(27), 9995 (2013)

82. H. Nasution, E. Purnama, S. Kosela, and J. Gunlazuardi, Photocatalytic reduction of CO on copper-doped Titania catalysts prepared by improved-impregnation method, *Catal. Commun.* 6(5), 313 (2005)

83. P. Li, J. Xu, H. Jing, C. Wu, H. Peng, J. Lu, and H. Yin, Wedged N-doped CuO with more negative conductive band and lower overpotential for high efficiency photoelectric converting CO_2 to methanol, *Appl. Catal. B* 156–157, 134 (2014)

84. N. Sagara, S. Kamimura, T. Tsubota, and T. Ohno, Photoelectrochemical CO_2 reduction by a p-type boron-doped g-C_3N_4 electrode under visible light, *Appl. Catal. B* 192, 193 (2016)

85. S. Liu, Z. R. Tang, Y. Sun, J. C. Colmenares, and Y. Xu, One-dimension-based spatially ordered architectures for solar energy conversion, *Chem. Soc. Rev.* 44(15), 5053 (2015)

86. N. P. Dasgupta, J. Sun, C. Liu, S. Brittman, S. C. Andrews, J. Lim, H. Gao, R. Yan, and P. Yang, Semiconductor nanowires – Synthesis, characterization, and applications, *Adv. Mater.* 26(14), 2137 (2014)

87. J. Le Xie, C. X. Guo, and C. M. Li, Construction of one-dimensional nanostructures on graphene for efficient energy conversion and storage, *Energy Environ. Sci.* 7(8), 2559 (2014)

88. A. I. Hochbaum and P. Yang, Semiconductor nanowires for energy conversion, *Chem. Rev.* 110(1), 527 (2010)

89. S. K. Choi, U. Kang, S. Lee, D. J. Ham, S. M. Ji, and H. Park, Sn-Coupled p-Si nanowire arrays for solar formate production from CO_2, *Adv. Energy Mater.* 4(11), 1301614 (2014)

90. S. Chu, S. Fan, Y. Wang, D. Rossouw, Y. Wang, G. A. Botton, and Z. Mi, Tunable syngas production from CO_2 and H_2O in an aqueous photoelectrochemical cell, *Angew. Chem. Int. Ed.* 55(46), 14262 (2016)

91. Q. Kong, D. Kim, C. Liu, Y. Yu, Y. Su, Y. Li, and P. Yang, Directed assembly of nanoparticle catalysts on nanowire photoelectrodes for photoelectrochemical CO_2 reduction, *Nano Lett.* 16(9), 5675 (2016)

92. G. Ghadimkhani, N. R. de Tacconi, W. Chanmanee, C. Janaky, and K. Rajeshwar, Efficient solar photoelectrosynthesis of methanol from carbon dioxide using hybrid CuO–Cu_2O semiconductor nanorod arrays, *Chem. Commun.* 49(13), 1297 (2013)

93. K. Rajeshwar, N. R. De Tacconi, G. Ghadimkhani, W. Chanmanee, and C. Janáky, Tailoring copper oxide semiconductor nanorod arrays for photoelectrochemical reduction of carbon dioxide to methanol, *ChemPhysChem* 14(10), 2251 (2013)

94. Q. Shen, Z. Chen, X. Huang, M. Liu, and G. Zhao, High-yield and selective photoelectrocatalytic reduction of CO_2 to formate by metallic copper decorated Co_3O_4 nanotube arrays, *Environ. Sci. Technol.* 49(9), 5828 (2015)

95. M. R. Khan, T. W. Chuan, A. Yousuf, M. N. K. Chowdhury, and C. K. Cheng, Schottky barrier and surface plasmonic resonance phenomena towards the photocatalytic reaction: Study of their mechanisms to enhance photocatalytic activity, *Catal. Sci. Technol.* 5(5), 2522 (2015)

96. Y. J. Jang, J. Jang, J. Lee, J. H. Kim, H. Kumagai, J. Lee, T. Minegishi, J. Kubota, K. Domen, and J. S. Lee, Selective CO production by Au coupled ZnTe/ZnO in the photoelectrochemical CO_2 reduction system, *Energy Environ. Sci.* 8(12), 3597 (2015)

97. J. S. DuChene, G. Tagliabue, A. J. Welch, W. H. Cheng, and H. A. Atwater, Hot hole collection and photoelectrochemical CO_2 reduction with plasmonic Au/p-GaN photocathodes, *Nano Lett.* 18(4), 2545 (2018)

98. J. Hou, H. Cheng, O. Takeda, and H. Zhu, Three-dimensional bimetal-graphene-semiconductor coaxial nanowire arrays to harness charge flow for the photochemical reduction of carbon dioxide, *Angew. Chem. Int. Ed.* 54(29), 8480 (2015)

99. G. Zeng, J. Qiu, Z. Li, P. Pavaskar, and S. B. Cronin, CO_2 reduction to methanol on TiO_2 -passivated GaP photocatalysts, *ACS Catal.* 4(10), 3512 (2014)

100. T. Hisatomi, J. Kubota, and K. Domen, Recent advances in semiconductors for photocatalytic and photoelectrochemical water splitting, *Chem. Soc. Rev.* 43(22), 7520 (2014)

101. Y. W. Chen, J. D. Prange, S. Dühnen, Y. Park, M. Gunji, C. E. D. Chidsey, and P. C. McIntyre, Atomic layer-deposited tunnel oxide stabilizes silicon photoanodes for water oxidation, *Nat. Mater.* 10(7), 539 (2011)

102. D. V. Esposito, I. Levin, T. P. Moffat, and A. A. Talin, H_2 evolution at Si-based metal–insulator–semiconductor photoelectrodes enhanced by inversion channel charge collection and H spillover, *Nat. Mater.* 12(6), 562 (2013)

103. B. Seger, T. Pedersen, A. B. Laursen, P. C. K. Vesborg, O. Hansen, and I. Chorkendorff, Using TiO_2 as a conductive protective layer for photocathodic H_2 evolution, *J. Am. Chem. Soc.* 135(3), 1057 (2013)

104. L. Ji, M. D. McDaniel, S. Wang, A. B. Posadas, X. Li, H. Huang, J. C. Lee, A. A. Demkov, A. J. Bard, J. G. Ekerdt, and E. T. Yu, A silicon-based photocathode for water reduction with an epitaxial $SrTiO_3$ protection layer and a nanostructured catalyst, *Nat. Nanotechnol.* 10(1), 84 (2015)

105. S. Xie, Q. Zhang, G. Liu, and Y. Wang, Photocatalytic and photoelectrocatalytic reduction of CO_2 using heterogeneous catalysts with controlled nanostructures, *Chem. Commun.* 52(1), 35 (2016)

106. B. Kumar, M. Llorente, J. Froehlich, T. Dang, A. Sathrum, and C. P. Kubiak, Photochemical and photoelectrochemical reduction of CO_2, *Annu. Rev. Phys. Chem.* 63(1), 541 (2012)

107. Y. Oh, and X. Hu, Organic molecules as mediators and catalysts for photocatalytic and electrocatalytic CO_2 reduction, *Chem. Soc. Rev.* 42(6), 2253 (2013)

108. J. Zhao, X. Wang, Z. Xu, and J. S. C. Loo, Hybrid catalysts for photoelectrochemical reduction of carbon dioxide: A prospective review on semiconductor/metal complex co-catalyst systems, *J. Mater. Chem. A* 2(37), 15228 (2014)

109. S. Bai, W. Yin, L. Wang, Z. Li, and Y. Xiong, Surface and interface design in cocatalysts for photocatalytic water splitting and CO_2 reduction, *RSC Advances* 6(62), 57446 (2016)

110. J. Yang, D. Wang, H. Han, and C. Li, Roles of cocatalysts in photocatalysis and photoelectrocatalysis, *Acc. Chem. Res.* 46(8), 1900 (2013)

111. W. Zhu, R. Michalsky, Ö. Metin, H. Lv, S. Guo, C. J. Wright, X. Sun, A. A. Peterson, and S. Sun, Monodisperse Au nanoparticles for selective electrocatalytic reduction of CO_2 to CO, *J. Am. Chem. Soc.* 135(45), 16833 (2013)

112. Q. Lu, J. Rosen, Y. Zhou, G. S. Hutchings, Y. C. Kimmel, J. G. Chen, and F. Jiao, A selective and efficient electrocatalyst for carbon dioxide reduction, *Nat. Commun.* 5(1), 3242 (2014)

113. D. Gao, H. Zhou, J. Wang, S. Miao, F. Yang, G. Wang, J. Wang, and X. Bao, Size-dependent electrocatalytic reduction of CO_2 over Pd nanoparticles, *J. Am. Chem. Soc.* 137(13), 4288 (2015)

114. F. Lei, W. Liu, Y. Sun, J. Xu, K. Liu, L. Liang, T. Yao, B. Pan, S. Wei, and Y. Xie, Metallic tin quantum sheets confined in graphene toward high-efficiency carbon dioxide electroreduction, *Nat. Commun.* 7(1), 12697 (2016)

115. M. Alvarez-Guerra, S. Quintanilla, and A. Irabien, Conversion of carbon dioxide into formate using a continuous electrochemical reduction process in a lead cathode, *Chem. Eng. J.* 207, 278 (2012)

116. K. P. Kuhl, E. R. Cave, D. N. Abram, and T. F. Jaramillo, New insights into the electrochemical reduction of carbon dioxide on metallic copper surfaces, *Energy Environ. Sci.* 5(5), 7050 (2012)

117. R. Long, Y. Li, Y. Liu, S. Chen, X. Zheng, C. Gao, C. He, N. Chen, Z. Qi, L. Song, J. Jiang, J. Zhu, and Y. Xiong, Isolation of Cu atoms in Pd lattice: Forming highly selective sites for photocatalytic conversion of CO_2 to CH_4, *J. Am. Chem. Soc.* 139(12), 4486 (2017)

118. S. Kaneco, H. Katsumata, T. Suzuki, and K. Ohta, Photoelectrocatalytic reduction of CO_2 in LiOH/methanol at metal-modified p-InP electrodes, *Appl. Catal. B* 64(1–2), 139 (2006)

119. R. Hinogami, Y. Nakamura, S. Yae, and Y. Nakato, An approach to ideal semiconductor electrodes for efficient photoelectrochemical reduction of carbon dioxide by modification with small metal particles, *J. Phys. Chem. B* 102(6), 974 (1998)

120. T. E. Rosser, C. D. Windle, and E. Reisner, Electrocatalytic and solar-driven CO_2 reduction to CO with a molecular manganese catalyst immobilized on mesoporous TiO_2, *Angew. Chem. Int. Ed.* 55(26), 7388 (2016)

121. D. Guzmán, M. Isaacs, I. Osorio-Román, M. García, J. Astudillo, and M. Ohlbaum, Photoelectrochemical reduction of carbon dioxide on quantum-dot-modified electrodes by electric field directed layer-by-layer assembly methodology, *ACS Appl. Mater. Interfaces* 7(36), 19865 (2015)

122. S. K. Kuk, R. K. Singh, D. H. Nam, R. Singh, J. Lee, and C. B. Park, Photoelectrochemical reduction of carbon dioxide to methanol through a highly efficient enzyme cascade, *Angew. Chem. Int. Ed.* 56(14), 3827 (2017)

123. L. Chen, Z. Guo, X. G. Wei, C. Gallenkamp, J. Bonin, E. Anxolabéhère-Mallart, K. C. Lau, T. C. Lau, and M. Robert, Molecular catalysis of the electrochemical and photochemical reduction of CO_2 with earth-abundant metal complexes: Selective production of CO vs. HCOOH by switching of the metal center, *J. Am. Chem. Soc.* 137(34), 10918 (2015)

124. V. S. Thoi, N. Kornienko, C. G. Margarit, P. Yang, and C. J. Chang, Visible-light photoredox catalysis: Selective reduction of carbon dioxide to carbon monoxide by a nickel N-heterocyclic carbene–isoquinoline complex, *J. Am. Chem. Soc.* 135(38), 14413 (2013)

125. H. Takeda, H. Koizumi, K. Okamoto, and O. Ishitani, Photocatalytic CO_2 reduction using a Mn complex as a catalyst, *Chem. Commun.* 50(12), 1491 (2014)

126. J. Bonin, M. Robert, and M. Routier, Selective and efficient photocatalytic CO_2 reduction to CO using visible light and an iron-based homogeneous catalyst, *J. Am. Chem. Soc.* 136(48), 16768 (2014)

127. K. Alenezi, S. K. Ibrahim, P. Li, and C. J. Pickett, Solar fuels: Photoelectrosynthesis of CO from CO_2 at p-type Si using Fe porphyrin electrocatalysts, *Chem.-Eur. J.* 19(40), 13522 (2013)

128. H. Rao, L. C. Schmidt, J. Bonin, and M. Robert, Visible-light-driven methane formation from CO_2 with a molecular iron catalyst, *Nature* 548(7665), 74 (2017)

129. I. Taniguchi, B. Aurian-Blajeni, and J. O. Bockris, The mediation of the photoelectrochemical reduction of carbon dioxide by ammonium ions, *J. Electroanal. Chem. Interfacial Electrochem.* 161(2), 385 (1984)

130. M. Szklarczyk, On the dielectric breakdown of water: An electrochemical approach, *J. Electrochem. Soc.* 136(9), 2512 (1989)

131. D. H. Won, J. Chung, S. H. Park, E. Kim, and S. I. Woo, Photoelectrochemical production of useful fuels from carbon dioxide on a polypyrrole-coated p-ZnTe photocathode under visible light irradiation, *J. Mater. Chem. A* 3(3), 1089 (2015)

132. A. Bachmeier, V. C. C. Wang, T. W. Woolerton, S. Bell, J. C. Fontecilla-Camps, M. Can, S. W. Ragsdale, Y. S. Chaudhary, and F. A. Armstrong, How light-harvesting semiconductors can alter the bias of reversible electrocatalysts in favor of H_2 production and CO_2 reduction, *J. Am. Chem. Soc.* 135(40), 15026 (2013)

133. A. Bachmeier, S. Hall, S. W. Ragsdale, and F. A. Armstrong, Selective visible-light-driven CO_2 reduction on a p-type dye-sensitized NiO photocathode, *J. Am. Chem. Soc.* 136(39), 13518 (2014)